Desalination and Water Treatment
www.deswater.com

doi: 10.5004/dwt.2023.29982

312 (2023) 100–107
November

Equilibrium and kinetic studies on adsorption of hexavalent chromium from aqueous solutions using solid-state iron exchange bentonite

Negin Abnous[a], Mohammad Ghorbanpour[b,*], Keivan Shayesteh[a]

[a]*Department of Chemical Engineering, University of Mohaghegh Ardabili, Ardabil, emails: abnosnegin@yahoo.com (N. Abnous), k.shayesteh@uma.ac.ir (K. Shayesteh)*
[b]*Department of Chemical Engineering, University of Tabriz, Tabriz, email: Ghorbanpour@uma.ac.ir*

Received 26 June 2023; Accepted 10 September 2023

ABSTRACT

The adsorption of hexavalent chromium by bentonite has been improved using solid-state iron exchange method. To understand the adsorption mechanisms and characteristics of parent bentonite and solid-state iron exchanged bentonite (SSIEB), various techniques including X-ray diffraction, Brunauer–Emmett–Teller analysis, Fourier-transform infrared spectroscopy, scanning electron microscopy, and energy-dispersive X-ray spectroscopy were employed. The results revealed that iron ions replaced some of the calcium and magnesium in bentonite during solid-state ion exchange, but no significant changes in morphology were observed. The d-spacing of the montmorillonite changed from 14.90 Å in the parent bentonite to 14.50, 14.60, and 14.90 Å for iron-exchanged bentonite prepared in 1, 3, and 5 min, respectively. The surface area increased from 44.5 m^2/g for bentonite to higher values (51.3–53.1 m^2/g) due to the solid-state iron exchange process. The chromate ion adsorption from aqueous solution increased from 5.61% to 18.85% for the sample synthesized at a temperature of 100°C and a time of 3 min. Consequently, the chromate adsorption capacity of the optimal SSIEB was nearly three times higher than that of pure bentonite. The data obtained from the solid-phase ion exchange method demonstrate that modified SSIEB can serve as an effective adsorbent in the absorption process.

Keywords: Chromium; Adsorption; Solid state; Iron exchange; Bentonite

1. Introduction

Drinking water contamination with chromium is one of the most important global health concerns due to its stability and relative toxicity [1]. Hexavalent chromium ions, $Cr_2O_7^{2-}$, have the potential to cause serious harm to the environment. Chromium release to water bodies is regulated at about 0.05 mg/L, while total chromium is regulated below 2.0 mg/L [1–3]. Today, various adsorbents including clay [4], activated carbon [5], alumina [6], silica [7], and zeolite [8] have been used to remove chromium from solutions [9]. Meanwhile, bentonite has special advantages such as inexpensiveness, biocompatibility, abundance, chemical stability, high adsorption capacity, and ion exchange capability [10–12]. Bentonite is a montmorillonite clay containing layered silicates. These layers consist of an octahedral alumina sheet placed between two tetrahedral silica sheets [13]. Surface alteration occurs due to the isomorphic replacement of central atoms in octahedra/tetrahedra by smaller valence cations, leading to changes in surface of the clay [14]. Consequently, the surface of the clay can adsorb positively charged ions through electrostatic interaction [15]. Thus, according to the characteristics and properties of absorbed cations, the surface charge of bentonite can be changed or new functional groups can be introduced to it [13]. The modified clays such as pillared bentonite [16,17],

* Corresponding author.

cation-exchanged bentonite [18,19], and bentonite modified with surfactant [20] have been developed and can serve as catalysts or efficient adsorbents for the treatment of various organic pollutants and minerals.

One of the simplest and most effective methods for modifying bentonite is solid-phase ion exchange, which involves the exchange of the exchangeable cation of bentonite and a suitable cation. This process is simple, fast, and highly effective. In this method, clay and a suitable salt are mixed and heated at a temperature close to the melting point of the salt. The molten salt infiltrates the clay's pores, facilitating cation exchange in the molten salt environment. Solid-state iron exchanged bentonite (SSIEB) has found applications in various fields. For instance, Ulhaq et al. [21] synthesized bentonite/copper catalysts using solid-phase ion exchange as heterogeneous catalysts for photo Fenton treatment of methyl orange under UV irradiation. In other studies, solid-state cation exchange has been employed to synthesize zinc, copper or silver-exchanged bentonite as antibacterial or photocatalytic materials [21,22]. Furthermore, solid-phase iron-exchanged bentonite has been utilized for the adsorption of dye from edible oil or solution [23,24]. However, to the best of our knowledge, using this adsorbent for heavy metal adsorption such as chromium has not been reported to date.

2. Materials and methods

2.1. Materials and chemicals

The original bentonite, predominantly of composed of Ca-montmorillonite, was purchased from the Kanisaz Jam Company (Rasht, Iran). All the chemicals used were of analytical grade and were purchased from Merck Co., Germany. The stock Cr(VI) solution was prepared by dissolving potassium dichromate in de-ionized water. The pH of the solution was adjusted by adding either 0.1 mol/L of HCl or 0.1 mol/L of NaOH, and measured with pH changes during the reaction with a pH meter.

2.2. Preparation of the SSIEBs

The detailed methods of preparing the SSIEB have been described in our previous work [21,23]. To prepare SSIEBs, a mixture of 5 g of bentonite and 2.5 g of $FeCl_2{\cdot}xH_2O$ was thoroughly combined and then heated at 100°C for 1, 3 and 5 min. The resulting samples were labeled as solid-state iron exchanged bentonite for 1 min (SSIEB1), for 3 min (SSIEB3) and for 5 min (SSIEB5), respectively. The mixture was then appropriately washed with distilled water, filtered, and dried in an oven for 24 h at 50°C.

2.3. Adsorption of Cr by SSIEBs

Adsorption isotherms of Cr(VI) on bentonite and prepared SSIEBs were determined using a batch equilibrium method. In each experiment 0.1 g of adsorbent was mixed with 25 mL Cr(VI) solution (25 mg/L) at various initial concentrations. The adsorption experiments were conducted in a thermostatic shaker bath at 25°C ± 0.1°C for 120 min. After equilibrium, the suspension was centrifuged, and concentration of Cr(VI) in the supernatant was measured using a UV-Vis spectrophotometer at 540 nm. The adsorbed amount (q_e) was calculated based on the difference between the initial (C_0 (mg/L)) and equilibrium (C_e (mg/L)) concentration according to Eq. (1):

$$q_e = \frac{\left[\left(C_0 - C_e\right) \times V\right]}{m} \tag{1}$$

where V is the total volume of solution (mL), and m is the mass of adsorbent (g). In order to determine the optimal conditions for chromate adsorption, the initial concentration of chromate, initial pH of solution, and adsorbent dosage were evaluated at 5–40 mg/L, 3–9, 0.025–0.15, respectively.

2.4. Characterization

Scanning electron microscopy (SEM) and elemental dispersive X-ray spectroscopy were carried out with an LEO 1430VP instrument (Germany). Fourier-transform infrared spectroscopy (FTIR) assessed the functional groups influencing the adsorption process in the wave number of 400–4,000 cm^{-1}, using a PerkinElmer Spectrophotometer (USA). The X-ray diffraction (XRD) patterns of the samples were characterized using an X-ray diffractometer (Philips PW 1050, The Netherlands) with CuKα radiation (λ = 1.5418 Å, 40 kV and 30 mA, 2θ from 0° to 80° and 0.05° step). A Micromeritics Brunauer–Emmett–Teller (BET) surface area and porosity analyzer (Gemini 2375, Germany) was used to evaluate the products with N_2 adsorption/desorption at the constant temperature of 77 K in the relative pressure range of 0.05–1.00.

3. Results and discussion

3.1. Characterization

3.1.1. SEM images

The SEM image obtained from parent bentonite and SSIEB3 is shown in Fig. 1. The typical structure of bentonite can be observed in Fig. 1a. After ion exchange, there is no noticeable change in the apparent morphology of the bentonite. This is due diffusion of iron ions into the montmorillonite interlayers, which cannot be visualized by the electron microscopy equipment.

3.1.2. FTIR spectra

The FTIR spectra of parent bentonite and SSIEB3 are given in Fig. 2. The spectrum of the parent bentonite exhibits the bands at 3,430 and 3,642 cm^{-1}, which correspond to the H–OH vibration of the water molecules adsorbed on the sorbent surface and –OH stretching vibration bands of water molecules bonded to the Si–O surface. The spectral band at 1,654 cm^{-1} is related to the bending of the H–OH bond of water molecules, which is retained in the matrix. The strong band at 1,048 cm^{-1} illustrates the presence of the Si–O–Si group of the tetrahedral sheet. The bands corresponding to Al–Al–OH bending vibrations are observed at 917 cm^{-1}. Peaks at 840 and 732 cm^{-1} confirm the presence of quartz in the samples [24]. Compared to the parent bentonite, the position of the –OH stretching vibration band shifts from

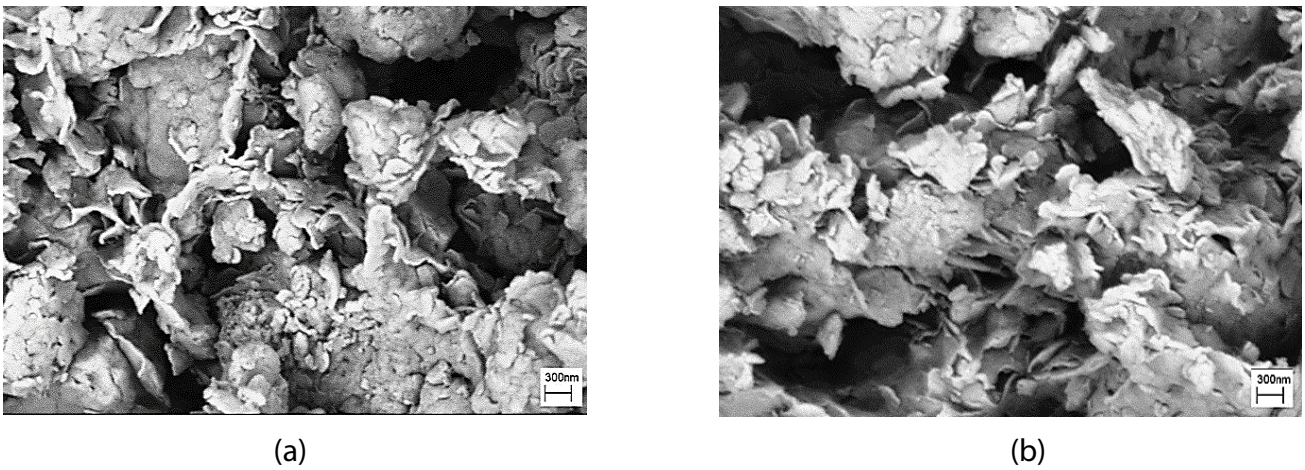

Fig. 1. Scanning electron microscopy image of parent bentonite (a) and SSIEB3 (b).

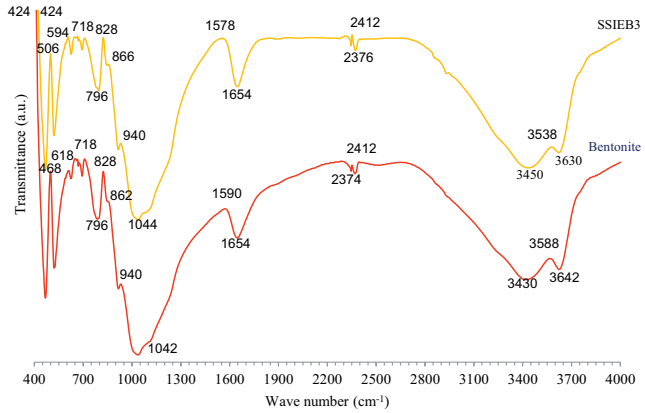

Fig. 2. Fourier-transform infrared spectra of parent bentonite and SSIEB3.

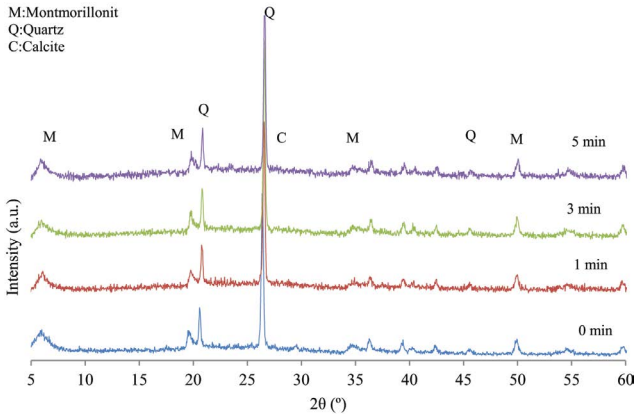

Fig. 3. X-ray diffraction patterns of parent bentonite and the ion exchanged samples (M: montmorillonite, Q: quartzes and C: calcite).

3,430 to 3,450 cm^{-1} in SSIEB3. In addition, significant changes were also detected for the relative band intensities in the region between 900 and 450 cm^{-1}. All those results reveal that ion exchange takes place successfully. In addition, it also confirms that this process maintains the basic composition of parent bentonite [25].

3.1.3. X-ray diffraction

Fig. 3 illustrates the XRD patterns of parent bentonite and SSIEB3. The XRD pattern of parent bentonite indicates the presence of montmorillonite (2θ = 5.6°, 19.5° and 49.9°) associated with quartzes (2θ = 20.8°, 26.2° and 49.9°) and calcite (2θ = 29.9°). As can be seen from Fig. 3, the diffraction peaks corresponding to the structure of bentonite existed in the XRD pattern of the ion-exchanged samples, which indicates that the montmorillonite structure remains intact after modification.

During solid-state ion exchange, the d-spacing calculated for the montmorillonite phase decreases from 14.90 Å in the parent bentonite to 14.50 Å for SSIEB1. According to available reports, this is due to water evaporation in the bentonite structure during the solid-phase ion exchange process [26]. By increasing the time of ion exchange to 3 and 5 min, the d-spacing increases to 14.60 and 14.90 Å, respectively. This is due to ion exchange and the presence of iron atoms with a larger size than cations existing in the interlayer space of bentonite. Relative changes in the peak positions and peak intensities in the ion-exchanged samples indicate that Fe atoms are well incorporated in the bentonite interlayers. In addition, no peaks in impurities were observed, indicating the high purity of the synthesized samples.

3.1.4. Elemental dispersive X-ray spectroscopy

The elemental composition of the parent bentonite and SSIEBs is present in Table 1. According to the results of Table 1, the existence of calcium, magnesium, and potassium in the interlayer structure of parent bentonite has been confirmed. Cations are responsible for connecting silicate layers. Compared to the parent bentonite, the ion-exchanged samples show an increase in iron content and a decrease in calcium, magnesium and potassium content. In other words, ion-exchanged samples do not contain any calcium, while bentonite contains it. It can be concluded that

the cation exchange has been conducted successfully. Finally, the amount of iron loaded increased significantly during the first minute and the changes made during the next minutes are less. This indicates the high penetration made during this process due to the use of heating during ion exchange.

3.1.5. Brunauer–Emmett–Teller

BET analysis of parent bentonite and SSIEBs is presented in Table 2. The surface area increases from 44.5 m^2/g for bentonite to higher amounts (between 51.3–53.1 m^2/g) as a consequence of the solid-state ion exchange process. This increase can be attributed to the formation of surface cracks and defects as a result of the collapse of the pore structure during this process.

3.2. Cr(VI) adsorption by various SSIEBs

The adsorption of Cr(VI) by SSIEBs and parent bentonite is shown in Fig. 4. It can be seen that, under identical conditions, the Cr(VI) adsorption by parent bentonite after 120 min was only 5.6%. The adsorption of Cr(VI) by SSIEB3 was 18.85%. The significantly increased adsorption of Cr(VI) by iron-exchanged bentonite may be related to the electrostatic interaction. It was reported that bentonite primarily consists of montmorillonite with the negatively charged surface, which is unfavorable for the adsorption of anionic chromate (CrO_4^{2-} and $HCrO_4^-$) due to electrostatic repulsion. After the ion-exchanged reaction, Fe-exchanged bentonite was obtained which contained higher positive charges, and could balance the surface charges of bentonite. Therefore, Fe-exchanged bentonite exhibited higher adsorption capacity for Cr(VI) anions in comparison with bentonite. This being so, more Cr(VI) anions can be enriched on the solid phase, facilitating the approach of Cr(VI) to the reactive sites of Fe-exchanged bentonite [27].

Table 1
Elemental composition of the parent bentonite and SSIEBs

Ion exchange time (min)	0	1	3	5
Oxygen	56.9	51.90	48.82	49.48
Magnesium	2.2	2.07	1.88	1.55
Aluminum	6.2	7.80	7.55	7.26
Silicon	29.8	33.30	37.21	36.10
Potassium	1.5	0.63	0.48	0.64
Iron	0.6	4.31	4.07	4.97
Calcium	2.8	0	0	0

Table 2
Brunauer–Emmett–Teller analysis of the parent bentonite and SSIEBs

Ion exchange time (min)	Surface area (m^2/g)	Cavity size (nm)	Cavity volume (cm^3/g)
0	44.5	1.66	0.067889
1	51.2	1.66	0.063881
3	53.1	1.22	0.066374
5	51.6	1.22	0.063757

3.2.1. Effect of initial pH

Fig. 5 shows the effect of pH on Cr(VI) adsorption by the optimally prepared sample, SSIEB3. The final Cr(VI) adsorption by SSIEB3 increased from 5.0% to 57.3% as the initial pH increased from 3.0 to 7.0. This indicates that the reduction of Cr(VI) by SSIEB3 is strongly pH dependent. At higher pH, the reduction of Cr(VI) decreases to 45.4%. The reactions for Cr(VI) are as follows:

$$H_2CrO_4 \Rightarrow HCrO_4^- + H^+ \quad (2)$$

$$HCrO_4^- + 7H^+ = Cr^{3+} + 4H_2O \quad (3)$$

$$HCrO_4^- \Rightarrow CrO_4^{-2} + H^+ \quad (4)$$

$$2HCrO_4^- \Rightarrow Cr_2O_7^{-2} + H_2O \quad (5)$$

The decrease in adsorption efficiency at low pH is caused by the adsorption competition between H^+ and Cr^{3+} species in solution. Conversely, at low pH values, many H^+ ions can adsorb and neutralize the negatively charged surface

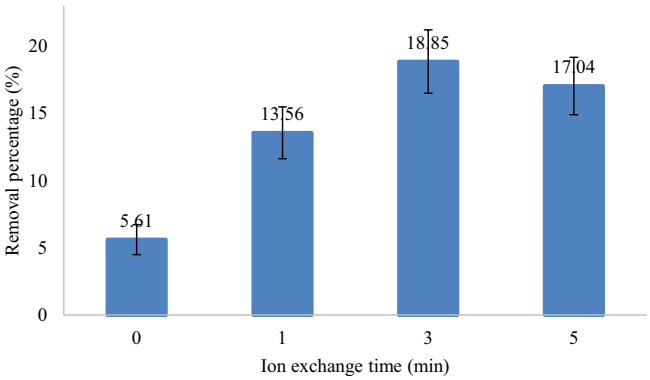

Fig. 4. Adsorption of Cr(VI) by SSIEBs and parent bentonite (50 mL, 9.85 ppm, pH = 5, 0.05 g/L).

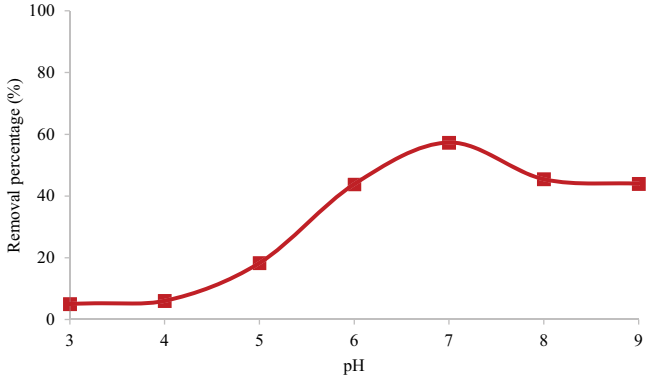

Fig. 5. Effect of pH on Cr(VI) adsorption by SSIEB3 (50 mL, 9.85 ppm, 0.05 g/L).

of the adsorbent [Eq. (3)]. With increasing pH, the concentration of available hydrogen ions decreases, and allowing more chromate is absorbed and the adsorption efficiency of Cr(VI) reaches a maximum [Eq. (4)]. However, with a further increase in pH, chromate turns into $Cr_2O_7^{2-}$ and bentonite releases absorbed hydrogen ions [Eq. (5)]. As a result, the surface of bentonite becomes more negative and the amount of absorption decreases. Atman et al. demonstrated that a pH range of 5–6 resulted in maximum uptake of heavy metals by bentonite [28–31]. In addition, the studies of Athman et al. [32] indicated that neutral pH is an ideal adsorption environment for metals by clay.

3.2.2. Effect of initial concentration

Fig. 6 presents the effect of the initial concentration of chromium(VI) on its adsorption by SSIEB3. The results showed that as initial concentration increases, the percentage of chromate adsorption decreases (Fig. 6a). This happens due to the saturation of the absorber. To facilitate better comparison, a graph of adsorption equilibrium vs. initial concentration (Fig. 6b) is also included. It illustrates that as the concentration of chromate solution increased, the equilibrium absorption (q_e) exhibits an upward trend. However, this upward trend stops as saturation is achieved at the concentration of 11.85 mg/L. At lower concentrations, there are more empty active sites and thus higher adsorption efficiency is expected. However, as the chromate concentration further increases, the adsorption efficiency decreases [33].

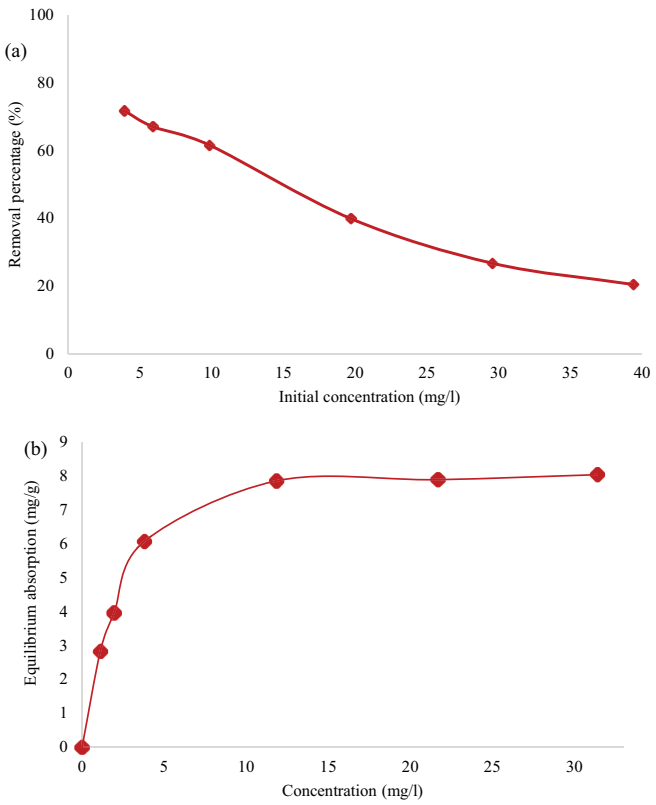

Fig. 6. Effect of initial concentration of Cr(VI) on its adsorption by SSIEB3 (50 mL, pH = 7, 0.05 g/L).

3.2.3. Effect of time

Fig. 7 shows the effect of time on Cr(VI) adsorption by SSIEB3. As observed in Fig. 6, the adsorption of Cr(VI) on SSIEB3 increases rapidly during the initial contact time of 5 min and then the sorption maintains a high level with increasing contact time. The kinetics of the sorption process can be divided into two distinct steps: an initial fast sorption, followed by a slow sorption. The quick Cr(VI) sorption rate at the beginning is attributed to the rapid diffusion of Cr(VI) from aqueous solutions to the external surfaces of SSIEB3. This can be explained on the basis that, initially a large number of vacant surface sites may be available for the adsorption of metal ions and over time, the surface sites become exhausted. The slow sorption process is attributed to the longer diffusion range of Cr(VI) into the inner-sphere pores of sorbent or the exchange with cations in the inner surface of SSIEB3 [34]. In this study, two pseudo-first-order and pseudo-second-order synthetic models were used for data analysis. These models are represented by Eqs. (6) and (7):

$$\log\left(q_e - q_t\right) = \log\left(q_e\right) - \frac{k_1}{2.303}t \tag{6}$$

$$\frac{t}{q_t} = \frac{1}{k_2 q_e^2} + \frac{1}{q_e}t \tag{7}$$

where k_1 (min^{-1}) is the adsorption rate constant, q_e, and q_t (mg/g) are the adsorption capacity of the adsorbent at equilibrium time, t(s) is the time, and k_2 (g/mg·min) is the adsorption rate constant. Fig. 8 shows the conformation of the experimental data with the pseudo-second-order model. The results are summarized in Table 3. The correlation coefficients (R^2) of the pseudo-second-order rate equation for the linear plot are very close to one, indicating that the kinetic sorption of Cr(VI) can be well described by the pseudo-second-order rate equation [35]. The q values for the optimal adsorbent from the pseudo-second-order equation were equal to 15.41 mg/g and the k value was equal to 0.0773 g/mg·min. The pseudo-second-order kinetic model is based on the assumption that the rate-limiting step is chemical sorption or chemisorption and predicts the behavior

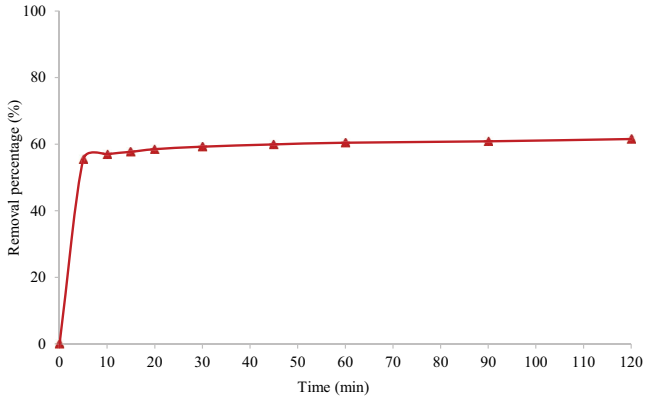

Fig. 7. Effect of contact time on Cr(VI) adsorption by SSIEB3 (50 mL, 9.85 ppm, pH = 7, 0.05 g/L).

over the whole range of adsorption. In this condition, the adsorption rate is dependent on adsorption capacity not on concentration of adsorbate [36].

3.2.4. Effect of adsorbent dosage

The percentage of Cr(VI) ion adsorption onto SSIEB3 was investigated at different adsorbent dosages in range 0.016–0.15 g/L (Fig. 9). Adsorbent concentration represents the number of adsorption sites available for removing the chromate from the aqueous solution. The number of active sites for chromate absorption has increased by keeping the parameters mentioned above constant and increasing the adsorbent dosages. The adsorption percentage increased sharply when the adsorbent dosages changed from 0.016 to 0.05 g/L. Subsequently, as the adsorbent dosage increased from 0.05 to 0.1 g/L, the adsorption percentage showed a gentle slope, suggesting a reduction in available chromate. Eventually, the absorption percentage reached equilibrium and remained uniform from the dosage of 0.1–0.15 g/L, without further increase. This is due to the balance between the absorbent and chromate. Therefore, an adsorbent dosage of 0.05 g/L was considered optimal.

3.2.5. Isotherms

To evaluate the sorption capacity of the sample, the sorption of Cr(VI) by SSIEB3 was carried out. In order to gain a better understanding of the mechanism and quantify the sorption data, the Langmuir and Freundlich models were adopted to fit the experimental sorption data. Freundlich equation is used for heterogeneous systems, irreversible adsorption systems, and non-monolayer adsorption. Its linear form can be expressed by Eq. (8):

$$\frac{C_e}{q_e} = \frac{1}{q_m K_l} + \frac{C_e}{q_m} \tag{8}$$

where q_{max}, is the maximum sorption capacity (mg/g), and b (L/mg) is the Langmuir constant. In comparison, the Langmuir adsorption isotherm is suitable for surface adsorption and homogeneous monolayer adsorption [37,38]. The Langmuir isotherm model is a theoretical model used to describe the monolayer sorption process onto a surface. The linear model can be represented by Eq. (9):

$$\log q_e = \log k_f + \left(\frac{1}{n}\right) \log C_e \tag{9}$$

where k_f and n are Freundlich constants. The obtained isotherm for Cr(VI) adsorption is shown in Fig. 10. From the correlation coefficients (R^2) (Table 4), one can see that the

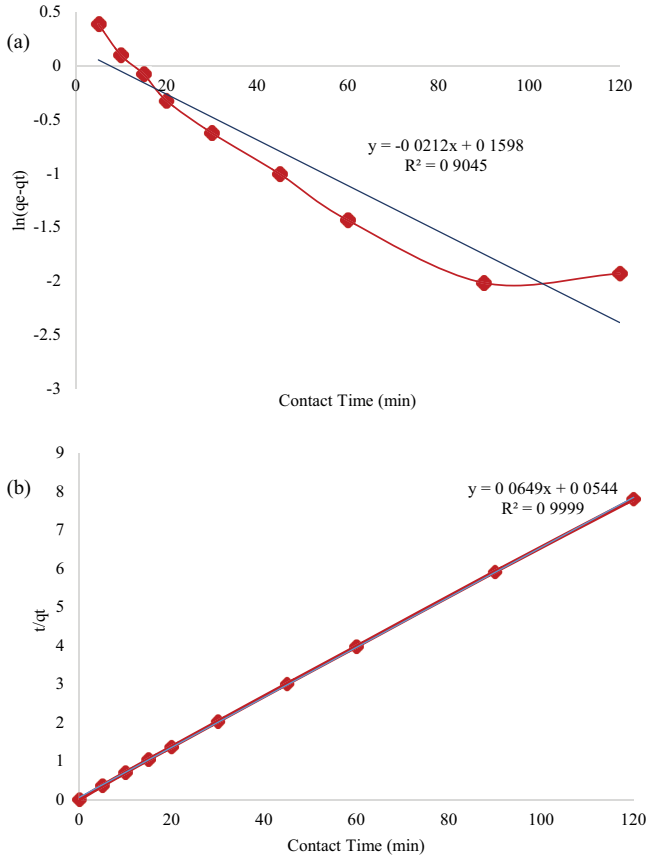

Fig. 8. Kinetic studies of Cr(VI) adsorption: pseudo-first-order (a) and pseudo-second-order (b) models.

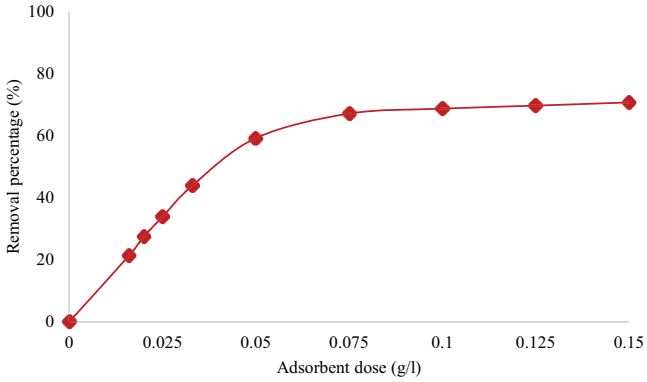

Fig. 9. Effects of the adsorbents dosage on the Cr(VI) adsorption by SSIEB3 (50 mL, 9.85 ppm, pH = 7).

Table 3
Parameter values of pseudo-first-order and pseudo-second-order models

Adsorbent	Pseudo-first-order			Pseudo-second-order		
	q_e	k_1 (h^{-1})	R^2	q_e	k_2 ($mg/m^2 \cdot h$)	R^2
FeB	1.2814	–0.00022	0.9629	15.4107	0.0773	0.9999

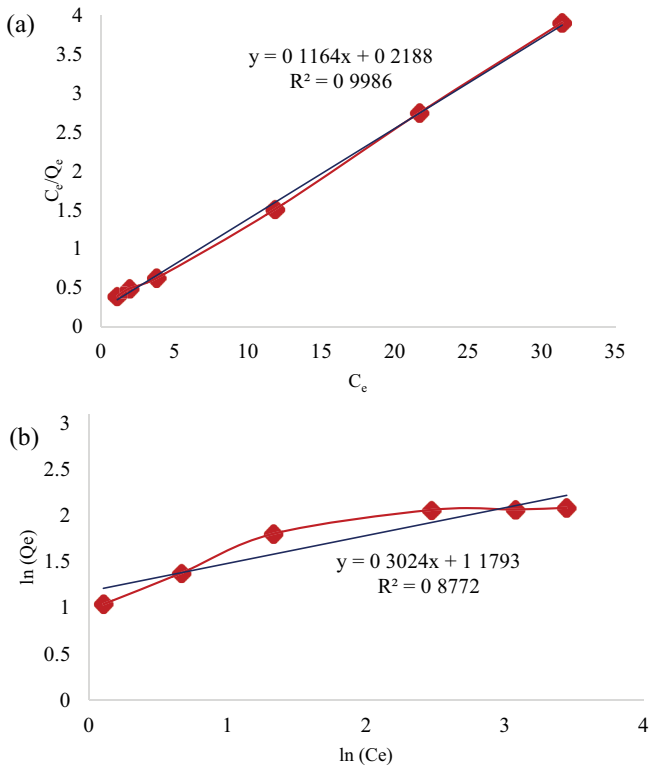

Fig. 10. Langmuir (a) and Freundlich (b) isotherms for Cr(VI) adsorption by SSIEB3 (50 mL, 9/85 ppm, pH = 7).

Table 4
Estimated parameters for the Langmuir and Freundlich models

Adsorbent	Langmuir constants			Freundlich constants		
	q_m (mg/g)	k_l (L/mg)	R^2	k_f (mg/g) (L/mg)	$1/n$	R^2
SSIEB3	4.57	1.87	0.9986	15.11	3.30	0.8776

Langmuir model (0.998) fits the sorption data better than the Freundlich model (0.877), which indicates that monolayer sorption occurs.

4. Conclusions

bentonite absorbed 5.61% of the chromate ion present in the aqueous solution. Among the samples synthesized by the ion exchange method at different times, the sample synthesized at 100°C and 3 min had the highest surface absorption and was selected as the optimal sample. Therefore, ion exchange with iron increased the chromate adsorption capacity by approximately 3.3 times compared to bentonite. The results revealed that iron ions replaced some of the calcium and magnesium in bentonite during solid-state ion exchange, but no significant changes in morphology were observed. The d-spacing of the montmorillonite changed from 14.90 Å in the parent bentonite to 14.50, 14.60, and 14.90 Å for iron-exchanged bentonite prepared in 1, 3, and 5 min, respectively. The surface area increased from 44.5 m^2/g for bentonite to higher values (51.3–53.1 m^2/g) due to the solid-state iron exchange process. The adsorption of chromate ions from the aqueous solution using the optimal synthesized sample was consistent with the pseudo-quadratic equation. The Langmuir adsorption model had a better correlation coefficient than the Freundlich model indicating the homogeneous surface of the desired adsorbent and, consequently, the uniformity of the available sites on the adsorbent surface. The data obtained from the ion exchange method in the solid phase showed that bentonite modified by this method can be used as an efficient adsorbent in the absorption process.

References

[1] A. Nezamzadeh-Ejhieh, H. Zabihi-Mobarakeh, Heterogeneous photodecolorization of mixture of methylene blue and bromophenol blue using CuO-nano-clinoptilolite, J. Ind. Eng. Chem., 20 (2014) 1421–1431.
[2] U. Baig, R.A.K. Rao, A.A. Khan, M.M. Sanagi, M.A. Gondal, Removal of carcinogenic hexavalent chromium from aqueous solutions using newly synthesized and characterized polypyrrole–titanium(IV)phosphate nanocomposite, Chem. Eng. J., 280 (2015) 494–504.
[3] M.A. Renu, K. Singh, Heavy metal removal from wastewater using various adsorbents: a review, J. Water Reuse Desalin., 7 (2017) 387–419.
[4] M. Tauqeer, M.S. Ahmad, M. Siraj, A. Mohammad, O. Ansari, M.T. Baig, Nanocomposite Materials for Wastewater Decontamination, M. Oves, M. Ansari, M. Zain Khan, M. Shahadat, M.I. Ismail, Eds., Modern Age Wastewater Problems, Springer, Cham, 2020, pp. 23–46. https://doi.org/10.1007/978-3-030-08283-3_2
[5] L.-n. Shi, X. Zhang, Z.-l. Chen, Removal of chromium(VI) from wastewater using bentonite-supported nanoscale zero-valent iron, Water Res., 45 (2011) 886–892.
[6] D. Mohan, K.P. Singh, V.K. Singh, Trivalent chromium removal from wastewater using low cost activated carbon derived from agricultural waste material and activated carbon fabric cloth, J. Hazard. Mater., 135 (2006) 280–295.
[7] S.S. Thavamani, R. Rajkumar, Adsorption of Cr(VI), Cu(II), Pb(II) and Ni(II) from aqueous solutions by adsorption on alumina, Res. J. Chem. Sci., 2231 (2013) 606X.
[8] K. Choi, S. Lee, J.O. Park, J.-A. Park, S.-H. Cho, S.Y. Lee, J.H. Lee, J.-W. Choi, Chromium removal from aqueous solution by a PEI-silica nanocomposite, Sci. Rep., 8 (2018) 1438, doi: 10.1038/s41598-018-20017-9.
[9] G. Lv, Z. Li, W.T. Jiang, C. Ackley, N. Fenske, N. Demarco, Adsorption of Cr(VI) from water using Fe(II)-modified natural zeolite, Chem. Eng. Res. Des., 92 (2014) 384–390.
[10] Y. Ren, Y. Han, X. Lei, C. Lu, J. Liu, G. Zhang, B. Zhang, Q. Zhang, A magnetic ion exchange resin with high efficiency of removing Cr(VI), Colloids Surf., A, 604 (2020) 125279, doi: 10.1016/j.colsurfa.2020.125279.
[11] F. Wang, W. Yang, F. Zheng, Y. Sun, Removal of Cr(VI) from simulated and leachate wastewaters by bentonite-supported zero-valent iron nanoparticles, Int. J. Environ. Res. Public Health, 15 (2018) 2162, doi: 10.3390/ijerph15102162.
[12] C. Zou, W. Jiang, J. Liang, X. Sun, Y. Guan, Removal of Pb(II) from aqueous solutions by adsorption on magnetic bentonite, Environ. Sci. Pollut. Res., 26 (2019) 1315–1322.
[13] M. Shaban, M.R. Abukhadra, M.G. Shahien, S.S. Ibrahim, Novel bentonite/zeolite-NaP composite efficiently removes methylene blue and Congo red dyes, Environ. Chem. Lett., 16 (2018) 275–280.
[14] W.A. Muslim, S.K. Al-Nasri, T.M. Albayati, Evaluation of bentonite, attapulgite, and kaolinite as eco-friendly adsorbents in the treatment of real radioactive wastewater containing Cs-137, Prog. Nucl. Energy, 162 (2023) 104730, doi: 10.1016/j.pnucene.2023.104730.

[15] Y.S. Chang, P.I. Au, N.M. Mubarak, M. Khalid, P. Jagadish, R. Walvekar, E.C. Abdullah, Adsorption of Cu(II) and Ni(II) ions from wastewater onto bentonite and bentonite/GO composite, Environ. Sci. Pollut. Res., 27 (2020) 33270–33296.
[16] J.-S. Kwon, S.-T. Yun, J.-H. Lee, S.-O. Kim, H.Y. Jo, Removal of divalent heavy metals (Cd, Cu, Pb, and Zn) and arsenic(III) from aqueous solutions using scoria: kinetics and equilibria of sorption, J. Hazard. Mater., 174 (2010) 307–313.
[17] H. Xu, X. Hu, Y. Chen, Y. Li, R. Zhang, C. Tang, X. Hu, Cd(II) and Pb(II) absorbed on humic acid-iron-pillared bentonite: kinetics, thermodynamics and mechanism of adsorption, Colloids Surf., A, 612 (2021) 126005, doi: 10.1016/j.colsurfa.2020.126005.
[18] H. Najafi, S. Farajfaed, S. Zolgharnian, S.H.M. Mirak, N. Asasian-Kolur, S. Sharifian, A comprehensive study on modified-pillared clays as an adsorbent in wastewater treatment processes, Process Saf. Environ. Prot., 147 (2021) 8–36.
[19] N.A.A. Qasem, R.H. Mohammed, D.U. Lawal, Removal of heavy metal ions from wastewater: a comprehensive and critical review, npj Clean Water, 4 (2021) 36, doi: 10.1038/s41545-021-00127-0.
[20] H. Pouraboulghasem, M. Ghorbanpour, R. Shayegh, S. Lotfiman, Synthesis, characterization and antimicrobial activity of alkaline ion-exchanged ZnO/bentonite nanocomposites, J. Cent. South Univ., 23 (2016) 787–792.
[21] I. Ulhaq, W. Ahmad, I. Ahmad, M. Yaseen, M. Ilyas, Engineering TiO_2 supported CTAB modified bentonite for treatment of refinery wastewater through simultaneous photocatalytic oxidation and adsorption, J. Water Process Eng., 43 (2021) 102239, doi: 10.1016/j.jwpe.2021.102239.
[22] N. Hajipour, M. Ghorbanpour, M. Safajou-Jahankhanemlou, Synthesis and characterization of solid-state Fe-exchanged nano-bentonite and evaluation of methyl orange adsorption, Environ. Sci. Pollut. Res., 29 (2022) 49898–49907.
[23] A. Almahri, The solid-state synthetic performance of bentonite stacked manganese ferrite nanoparticles: adsorption and photo-Fenton degradation of MB dye and antibacterial applications, J. Mater. Res. Technol., 17 (2022) 2935–2949.
[24] R.G. Jajin, M. Ghorbanpour, Removal of asphaltene by solid-phase iron exchanged bentonite, Environ. Prog. Sustainable Energy, 42 (2023) e14032, doi: 10.1002/ep.14032.
[25] S. Minz, S. Garg, R. Gupta, Catalytic wet peroxide oxidation of 4-nitrophenol over Al–Fe, Al–Cu and Al–Cu–Fe pillared clays, Indian Chem. Eng., 60 (2018) 16–36.
[26] M. Marciniak, J. Goscianska, M. Norman, T. Jesionowski, A. Bazan-Wozniak, R. Pietrzak, Equilibrium, kinetic, and thermodynamic studies on adsorption of Rhodamine B from aqueous solutions using oxidized mesoporous carbons, Materials, 15 (2022) 5573, doi: 10.3390/ma15165573.
[27] A. Nouri, M. Ghorbanpour, S. Lotfiman, 2018. Diffusion of Cu ions into nanoclay by molten salt ion exchange for antibacterial application, J. Phys. Sci., 29 (2018) 31–42.
[28] L. Ma, Y. Du, S. Chen, D. Du, H. Ye, T.C. Zhang, Highly efficient removal of Cr(VI) from aqueous solution by pinecone biochar supported nanoscale zero-valent iron coupling with *Shewanella oneidensis* MR-1, Chemosphere, 287 (2022) 132184, doi: 10.1016/j.chemosphere.2021.132184.
[29] T.M. Madumo, S.A. Zikalala, N.N. Gumbi, S.B. Mishra, B. Ntsendwana, E.N. Nxumalo, Development of nitrogen-doped graphene/MOF nanocomposites towards adsorptive removal of Cr(VI) from the wastewater of the Herbert Bickley treatment works, Environ. Nanotechnol. Monit. Manage., 20 (2023) 100794, doi: 10.1016/j.enmm.2023.100794.
[30] M. Kondalkar, U. Fegade, Inamuddin, S. Kanchi, T. Altalhi, E.K. Suryawanshi, A.M. Patil, Adsorption of Cr(VI) on ultrafine Al_2O_3-doped $MnFe_2O_4$ nanocomposite surface: experimental and theoretical study using double-layer modeling, J. Phys. Chem. Solids, 163 (2022) 110544, doi: 10.1016/j.jpcs.2021.110544.
[31] H. Niu, H. Yang, L. Tong, A.R. Kamali, The adsorption characteristics and performance of gold onto elemental carbon extracted from refractory carbonaceous gold concentrate, Colloids Surf., A, 658 (2023) 130635, doi: 10.1016/j.colsurfa.2022.130635.
[32] S. Athman, A. Sdiri, M. Boufatit, Spectroscopic and mineralogical characterization of bentonite clay (Ghardaïa, Algeria) for heavy metals removal in aqueous solutions, Int. J. Environ. Res., 14 (2019) 1–14, doi: 10.1007/s41742-019-00232-6.
[33] A. Sdiri, T. Higashi, F. Jamoussi, S. Bouaziz, Effects of impurities on the removal of heavy metals by natural limestones in aqueous systems, J. Environ. Manage., 93 (2012) 245–253.
[34] N.S. Topare, V.S. Wadgaonkar, A review on application of low-cost adsorbents for heavy metals removal from wastewater, Mater. Today Proc., 77 (2023) 8–18.
[35] K. Oukebdane, I. Lacene Necer, M.A. Didi, Binary comparative study adsorption of anionic and cationic azo-dyes on Fe_3O_4-bentonite magnetic nanocomposite: kinetics, equilibrium, mechanism and thermodynamic study, Silicon, 14 (2022) 9555–9568.
[36] Ş. İrdemez, G. Durmuş, S. Kul, F.E. Torun, Z. Bingül, Comparison of kinetics of Cr(III) ions removal from wastewater using raw and activated montmorillonite minerals, EQA – Int. J. Environ. Qual., 45 (2021) 17–26.
[37] B. An, Cu(II) and As(V) adsorption kinetic characteristic of the multifunctional amino groups in chitosan, Processes, 8 (2020) 1194, doi: 10.3390/pr8091194.
[38] S. Srivastava, S.B. Agrawal, M.K. Mondal, Biosorption isotherms and kinetics on removal of Cr(VI) using native and chemically modified *Lagerstroemia speciosa* bark, Ecol. Eng., 85 (2015) 56–66.